Report

Current Biology

Nanostructures and Monolayers of Spheres Reduce Surface Reflections in Hyperiid Amphipods

Highlights

- The appendages of the hyperiid *Cystisoma* have arrays of cuticular nanoprotuberances
- The cuticles of seven hyperiid species have monolayers of subwavelength-sized spheres
- Both features reduce surface reflections from these transparent oceanic species

Authors

Laura E. Bagge, Karen J. Osborn, Sönke Johnsen

Correspondence

laura.elizabeth.bagge@gmail.com

In Brief

Bagge et al. use microscopy and optical modeling to show that hyperiid amphipods (oceanic crustaceans that are mostly transparent) have two previously undocumented features—cuticular nanoprotuberances and monolayers of subwavelength-sized spheres—that reduce their surface reflections, making their cuticle less visible to potential predators.

Bagge et al., 2016, Current Biology *26*, 1–6
November 21, 2016
http://dx.doi.org/10.1016/j.cub.2016.09.033

CellPress

Please cite this article in press as: Bagge et al., Nanostructures and Monolayers of Spheres Reduce Surface Reflections in Hyperiid Amphipods, Current Biology (2016), http://dx.doi.org/10.1016/j.cub.2016.09.033

Current Biology
Report

Nanostructures and Monolayers of Spheres Reduce Surface Reflections in Hyperiid Amphipods

Laura E. Bagge,[1,3,*] Karen J. Osborn,[2] and Sönke Johnsen[1]
[1]Biology Department, Duke University, Box 90338, Durham, NC 27708, USA
[2]Department of Invertebrate Zoology, Smithsonian National Museum of Natural History, Washington, DC 20013, USA
[3]Lead Contact
*Correspondence: laura.elizabeth.bagge@gmail.com
http://dx.doi.org/10.1016/j.cub.2016.09.033

SUMMARY

Transparent zooplankton and nekton are often nearly invisible when viewed under ambient light in the pelagic zone [1–3]. However, in this environment, where the light field is directional (and thus likely to cause reflections), and under the bioluminescent searchlights of potential predators, animals may be revealed by reflections from their body surface [4–7]. We investigated the cuticle surfaces of seven species of hyperiids (Crustacea; Amphipoda) using scanning electron microscopy and found two undocumented features that may reduce reflectance. We found that the legs of *Cystisoma* spp. (n = 5) are covered with an ordered array of nanoprotuberances 200 ± 20 nm SD in height that function optically as a gradient refractive index material [6, 8, 9]. Additionally, we observed that *Cystisoma* and six other species of hyperiids are covered with a monolayer of homogenous spheres (diameters ranging from 52 ± 7 nm SD on *Cystisoma* spp. to 320 ± 15 nm SD on *Phronima* spp.). Optical modeling using effective medium theory and transfer matrix methods demonstrated that both the nanoprotuberances and the monolayers reduce reflectance by as much as 100-fold, depending on the wavelength and angle of the incident light and the thickness of the gradient layer. Even though we only consider surface reflectance and not internal light scattering, our study demonstrates that these nanoprotuberances and spheres can improve crypsis in a featureless habitat where the smallest reflection can render an animal vulnerable to visual predation.

RESULTS AND DISCUSSION

Amphipods in the suborder *Hyperiidea* inhabit oceanic waters from the surface to over 4,000 m deep [10, 11]. In this environment, transparent animals, especially those with higher refractive index surfaces, such as hyperiids, may be under selective pressure to minimize their surface reflections because the blue-green downward radiance is at least two orders of magnitude greater than horizontal radiance at all depths [5, 6]. Thus, even reflection of only 1% of this downward light into the horizontal plane can significantly increase the contrast of an otherwise cryptic animal.

Light is reflected and refracted at interfaces between materials with different refractive indices, in this case, from seawater (refractive index [RI] = 1.34) to the hyperiid's chitinous cuticle (RI = 1.57) [12, 13]. This reflectance can be minimized by altering the gradient in refractive index between seawater and the cuticle so that the transition is less abrupt [6, 8, 9]. This can be accomplished by (1) having an ordered array of subwavelength nanoprotuberances or (2) having a thin film with an index that is between that of the seawater and the cuticle. We examined seven hyperiid species (representing six families) that appeared transparent and/or red in coloration and ranged in body length from 10 mm to >100 mm (Figure S1) to determine whether they possess any features that alter the index gradient. Using scanning electron microscopy (SEM), we observed both ordered arrays of cuticular nanoprotuberances and previously undescribed dense monolayers of spheres that appear to be bacteria, at least in some cases (Figure 1). We then used transfer matrix methods [14] to show that these structures reduce surface reflectance by as much as 100-fold. In most cases, there was an absolute reduction from ~1% reflectance to less than 0.1% reflectance (Figures 2 and 3).

Nanoprotuberances on Cystisoma

Subwavelength nanostructures, first observed on the corneal surface of the compound eyes of moths and butterflies [12, 16] and later found on the transparent wings of moths and cicadas [17, 18], have a geometry in which the fractional area of chitin increases as light approaches the insect's surface, resulting in a smoother gradient in refractive index and less reflected light [6, 8, 9]. How much reflectance is reduced depends on the shape of the gradient, the indices of both the medium and the surface, and the angle and wavelength of the incident light. Direct experimental evidence has previously demonstrated that theoretical models based on these morphological parameters accurately predict surface reflectances (e.g., [19, 20]).

We found that the legs of *Cystisoma* (the largest free-swimming hyperiid we examined) were 90%–100% covered from insertion point to distal tip on all sides by an ordered, periodic array of nanoprotuberances (Figure 1A). We measured 100 randomly sampled nanoprotuberances from each of the five *Cystisoma* specimens and found that they were 200 ± 20 nm SD high and spaced 96 ± 5 nm SD apart (or approximately 100

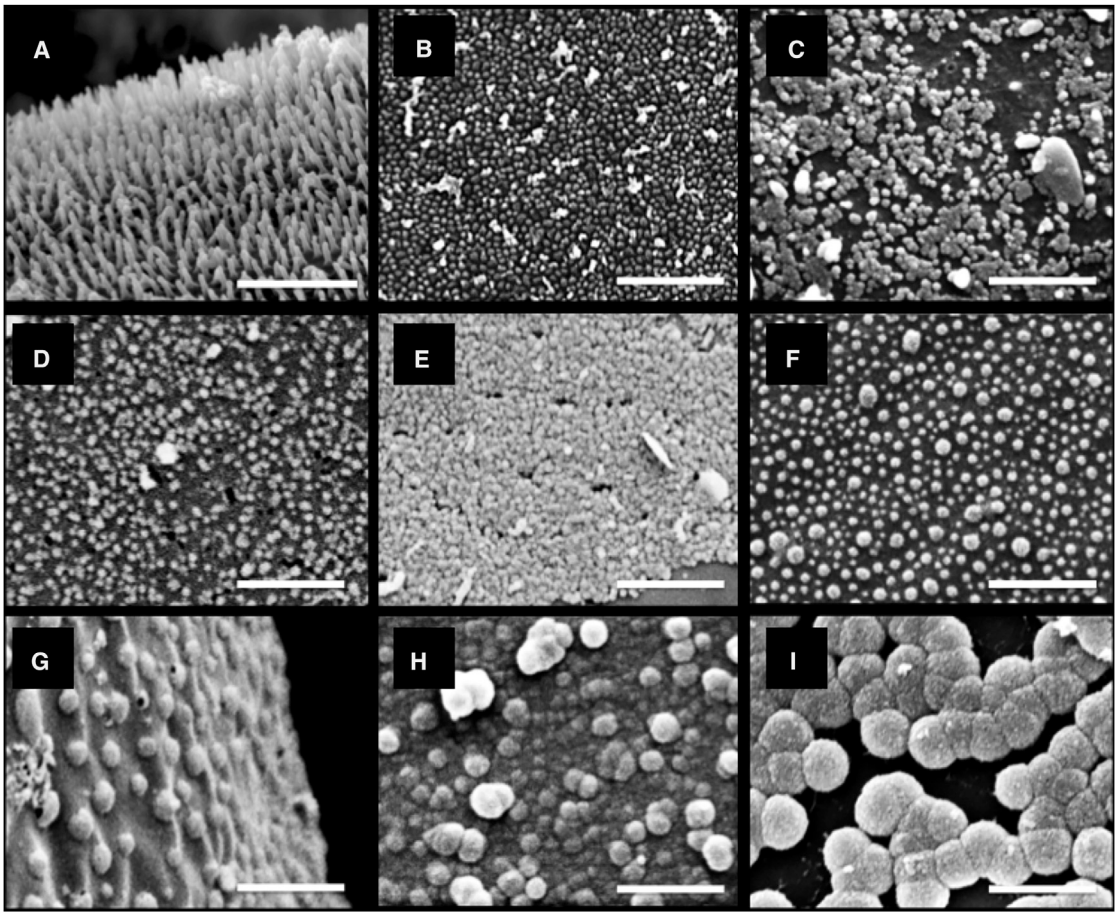

Figure 1. Scanning Electron Micrographs of the Cuticular Surfaces of Hyperiid Amphipods

(A) *Cystisoma* spp. (n = 5) appendages were covered by an ordered array of nanoprotuberances 200 ± 20 nm tall.

(B) *Cystisoma* sp. (n = 1) had dorsal and ventral surfaces covered with an ordered array of cuticular nanoprotuberances 50 ± 4 nm tall.

(C–H) Spheres of various diameter covering the body surfaces of hyperiids. (C) *Cystisoma* spp. (n = 5), 52 ± 7 nm diameter. (D) *Lanceola pelagica* (n = 2), 70 ± 9 nm diameter. (E) *Platyscelus armatus* (n = 2), 80 ± 10 nm diameter. (F) *Leptocotis* spp. (n = 3), 110 ± 25 nm diameter. (G) *Glossocephalus milneedwardsi* (n = 2), 220 ± 30 nm diameter. (H) *Paraphronima gracilis* (n = 2), 240 ± 25 nm diameter.

(I) *Phronima* spp. (n = 5), 320 ± 15 nm diameter.

The scale bars represent 1 μm. See Figure S1 for ex situ (maximized for visibility) photographs of hyperiids and Figure S2 for SEMs demonstrating coverage of the nanoprotuberances and spheres.

nanoprotuberances per μm^2). The base and tip diameters of each nanoprotuberance were 80 ± 4 nm SD and 25 ± 6 nm SD, respectively, making them similar in shape and size to structures found on the transparent wings of insects and eyes of moths [12–14, 16, 17]. One *Cystisoma* specimen in addition had nanoprotuberances on its dorsal body and extending onto its ventral surface approximately 1 mm beyond the leg insertions (Figure 1B).

Monolayers of Spheres

Reflectance can also be reduced by a thin layer composed of a substance with an intermediate refractive index that again smooths the index gradient between the medium and the surface [6, 8, 9]. If the index of this layer is the geometric mean of the medium and surface indices, then it abolishes all reflection for light with a wavelength (measured inside the layer) that is four times the thickness of the layer. Whereas human technology has taken advantage of thin layers for minimizing reflectance in lenses [6, 8, 9], no animal has been shown to use thin layers to reduce reflectance.

We observed that the cuticular surfaces of exemplars from seven different genera spanning the diversity of the Hyperiidea were covered with a dense organic monolayer of morphologically homogenous spheres, which appeared to be a monoculture of coccoid bacteria (Figures 1C–1I). X-ray diffraction analysis using a Philips XL30S FEG SEM on the thin layers did not reveal any inorganic components. Observing the cuticle surface from all specimens from a side angle and freeze fracturing the cuticle along its edge for *Phronima* and *Cystisoma* specimens showed that the spheres were not structures emerging from the cuticle itself. The spheres on *Phronima*, for instance, were instead attached to the cuticle with what appear to be fimbriae (Figure S2A). Many spheres showed what appear to be planes of binary fission (Figure S2B), again suggesting

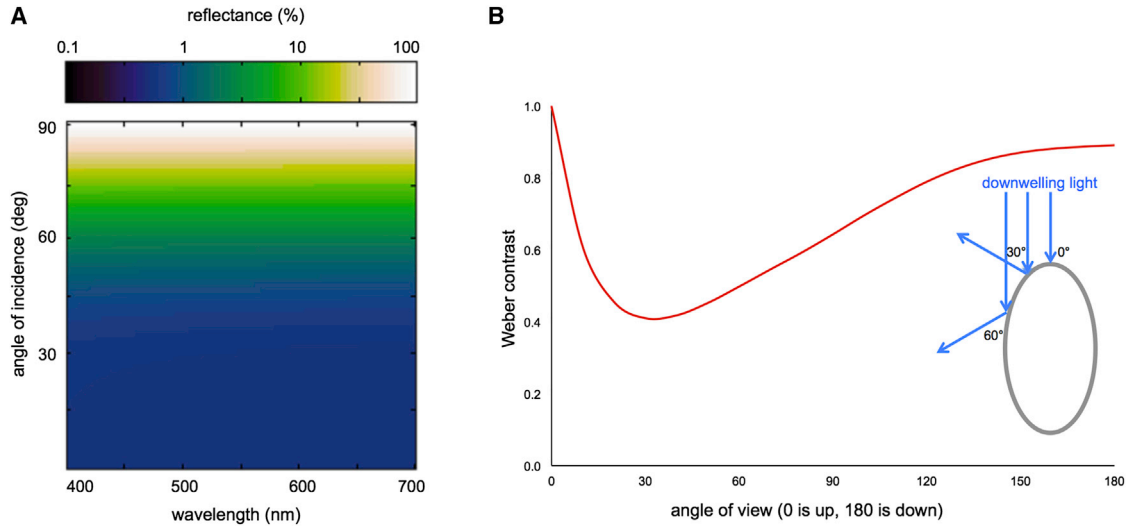

Figure 2. Reflectance of a Flat, Clean Hyperiid Cuticle

(A) Transfer matrix predictions of cuticle reflectance in seawater for a flat, clean, chitinous cuticle.

(B) The Weber contrast of flat, clean cuticle viewed at different angles (looking straight up to looking straight down), demonstrating that reflectance from the cuticle (values from A) may significantly increase the hyperiid's contrast and break camouflage. The wavelength of the incident light is assumed to be 480 nm, the depth is assumed to be greater than 200 m with a vertically symmetric light field, and we only consider reflections of the dominating downward radiance. Background radiance was calculated using measured inherent optical properties and radiative transfer software [5, 15]. The inset schematic visualizes these assumptions, showing downwelling light hitting a cuticle surface at different angles of incidence with 0° being perpendicular to the cuticle.

that at least some of these spheres are one or more species of nanobacteria.

Within each genus, we measured 100 randomly sampled spheres from each specimen and found that their diameters ranged from 52 ± 7 nm SD on *Cystisoma* (Figure 1C) to 320 ± 15 nm SD on *Phronima* (Figure 1I). The densest aggregations of spheres (>90% by area coverage) occurred at the joints between the body segments. Moderate-density (>40% coverage) monolayers were found on all body segments, and low-density (<20% coverage) monolayers were found on parts of the head or antennae (but not on the eyes; Figures 1 and S2).

Modeling Shows Reduced Cuticle Reflectance

To determine whether the nanoprotuberances and monolayers reduced reflectance, we used both effective medium and transfer matrix theory. We first modeled the reflectance from a clean, flat, chitinous surface in seawater over all angles of incidence (with 0° being perpendicular to the cuticle surface) and over all wavelengths of visible light (400–700 nm; Figure 2A). This showed that between 0.6% and 1% of incident light is reflected at angles of incidence less than 55°. Because reflectance depends strongly on the angle of incidence [6], reflectance is as much as 7% at 75° and 100% at 90° (Figure 2A). However, even 1% reflectance can cause a hyperiid to be distinguishable from the background (Figure 2B).

When we modeled how the nanoprotuberances on the appendages of *Cystisoma* affected cuticle reflectance (Figures 3A and 3B), we found reflectance was reduced to less than 0.5% over a broad range of wavelengths and angles of incidence (Figure 3A). Because dehydrating specimens for SEM may cause as much as 20% shrinkage of tissues [21], we performed a second set of calculations that assumed the nanoprotuberances were 20% wider than measured (Figures S3A and S3B). The modeled reflectance from these wider nanoprotuberances was less than 0.1% over certain angles of incidence (~60°–80°) and for 400–600 nm light (Figure S3A).

We also modeled how the different monolayer thicknesses affected cuticle reflectance (Figures 3C–3H and S3C–S3J). We treated the spheres as single layers dense enough to be touching or nearly touching with thicknesses of 52 nm, 110 nm, and 320 nm, respectively, and a refractive index of 1.44 [22] (Figures 3C–3H). We modeled several layer thicknesses to account for possible shrinkage during fixation and SEM preparation [23] and found that, even if the spheres were larger in situ, they still fell within the modeled range (Figures S3C–S3J). Similarly, we expect that animal handling reduced the numerical density of the spheres and that percent cover is higher in undisturbed specimens. The 52 nm layer of spheres did not reduce cuticle reflectance as much as the larger spheres, but cuticle reflectance was lowered to less than 0.5% at angles of incidence less than 45° between 400 nm and 500 nm wavelengths of light (Figure 3C). The 110 nm layer functioned the best, reducing cuticle reflectance to less than 0.1% over a broad range of wavelengths and angles of incidence, showing a more than 50-fold reduction in reflectance at 45° for 480 nm light (Figures 3E and 3F). The largest-sized 320 nm spheres also reduced cuticle reflectance to less than 0.1% for angles of incidence between 45° and 60° for blue-green (480 nm) light, with an approximately 50-fold reduction in reflectance (Figures 3G and 3H).

Importance of Reduced Cuticle Reflectance for Hyperiids

Our results suggest two mechanisms for minimizing surface reflectance in pelagic species. Nanoprotuberances and monolayers of

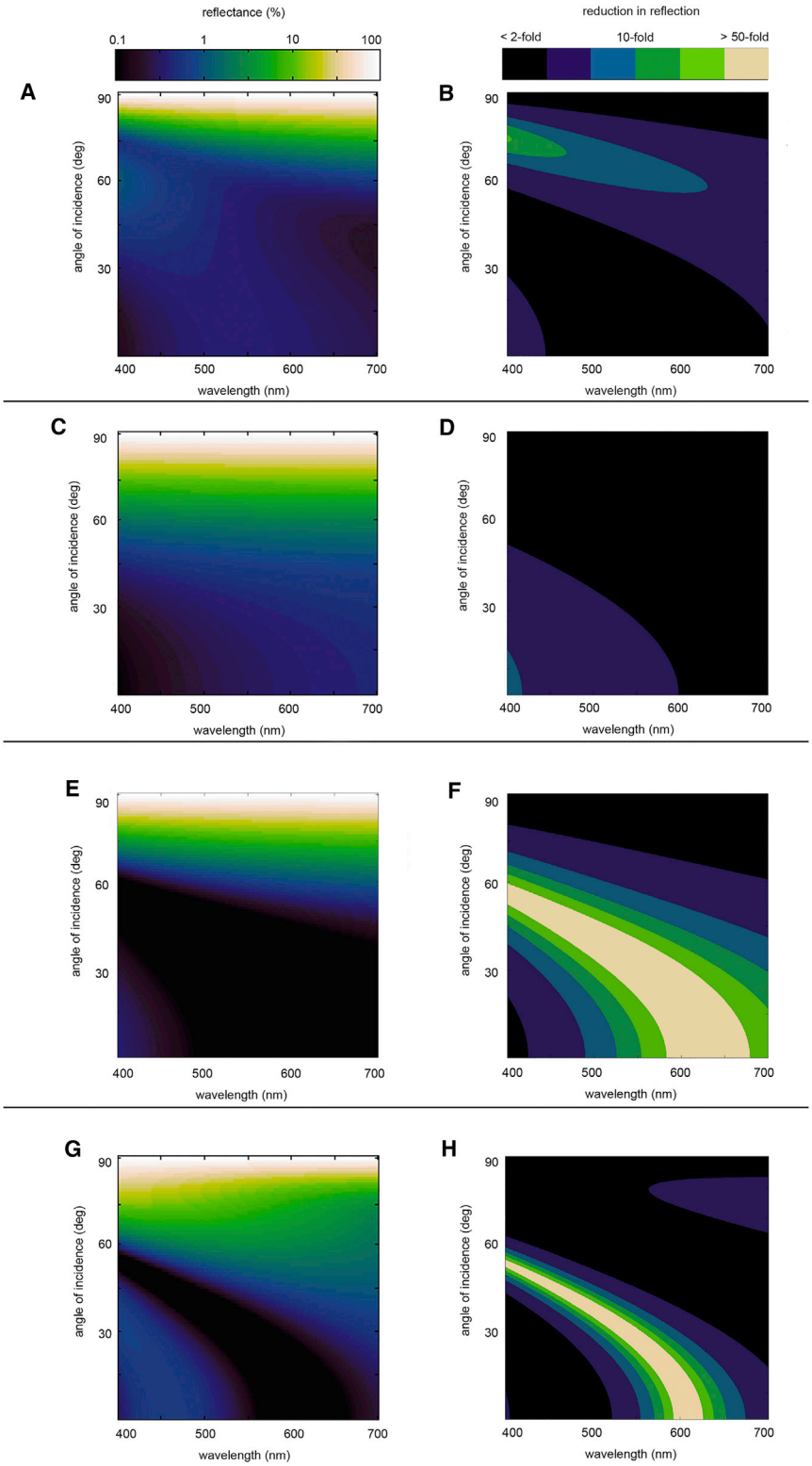

Figure 3. Transfer Matrix Predictions of Cuticle Reflectance in Seawater and the Reduction in Reflection as Compared to a Clean, Flat, Chitinous Cuticle

Transfer matrix predictions of cuticle reflectance in seawater (left) and the reduction in reflection as compared to a clean, flat, chitinous cuticle (right) for the nanoprotuberances on *Cystisoma* appendages (A and B), the 52-nm-thick layer found on the cuticle of *Cystisoma* (C and D), the 110-nm-thick layer found on the cuticle of *Leptocotis* (E and F), and the 320-nm-thick layer found on the cuticle of *Phronima* (G and H). See Figure S3 for additional predictions.

spheres both reduced reflectance of blue-green bioluminescence and ambient light by as much as 100-fold. In most cases, the absolute reflectance was reduced to 0.1% for blue-green light and angles of incidence less than 45° (Figure 3). We suggest that reducing surface reflectance from 1% to less than 0.1% may be important for camouflage, especially in cases where bioluminescent predators shine a searchlight on their hyperiid prey.

Whereas hyperiid amphipods traditionally were thought to be associated with gelatinous hosts [10, 11], we now know that some taxa are free swimming and may be an important food source for animals in higher trophic levels with good visual systems. In situ midwater observations show that cystisomatids and lanceolids are typically not observed in association with gelatinous animals (134 of 137 cystisomatid observations; 889 of 894 lanceolid observations; K.J.O., unpublished data); instead, it appears they spend their lives free swimming in the water column. Additionally, *Phronima* are observed free swimming (not associated with a salp barrel) in nearly 1/3 of in situ observations for which behavior was recorded (31 of 87 observations; K.J.O., unpublished data). The decrease in contrast due to the cuticular structures on the hyperiids may be enough to help hyperiids avoid detection by deep-water fish predators that have relatively good spatial acuity and contrast sensitivity (generally becoming sharper with depth and ranging from a low acuity of 1.3 cycles per degree in *Lampanyctus ater* to 22.9 cycles per degree in *Alepocephalus bairdii*) [24].

For all species of *Cystisoma* (the largest hyperiid, with body lengths over 100 mm), the legs make up a visible and large-moving portion of the entire animal. With few exceptions, we primarily found nanoprotuberances on only the appendages of *Cystisoma*. These appendages have many angles and edges that could increase the chance of the animal being seen, so we believe that the legs could especially benefit from having anti-reflective

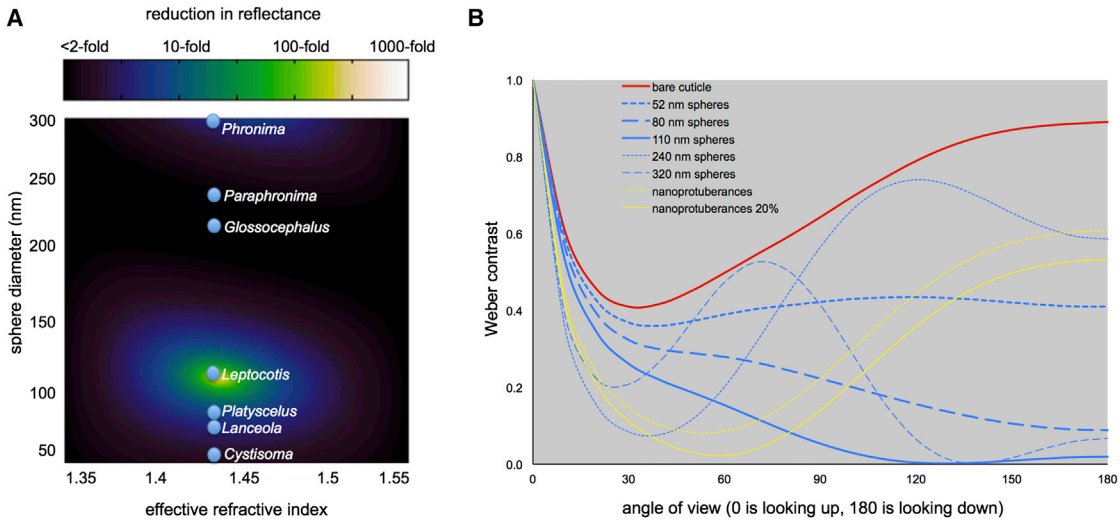

Figure 4. Models of the Effect of Cuticular Nanostructures and Spheres on Crypsis

(A) Reduction of reflectance as a function of sphere diameter and effective refractive index for 480 nm light incident at a 45° angle. The blue markers represent the seven species-specific measured diameters of the spheres.

(B) The Weber contrast of a hyperiid cuticle with the observed nanostructures and spheres and without (bare cuticle) for comparison. As in Figure 2B, light is assumed to have a narrow spectral distribution centered on 480 nm, and depth is assumed to be greater than 200 m with a vertically symmetric light field.

structures. Whereas our optical modeling showed that these nanoprotuberances reduce cuticle reflectance, we realize that they may also serve other functions, such as anti-fouling or prey capture.

We also acknowledge that the monolayers of spheres may be a by-product of living in an ocean surrounded by abundant nanoplankton rather than an adaptive symbiosis. Because we only examined adults and did not determine molt stage, we do not know whether monolayers are vertically transferred (seeded from prior cuticle) or re-acquired from the environment. However, whether or not the spheres are involved in a symbiosis, our micrographs show evidence of a previously unknown association. Research currently underway may confirm the identity of the monolayers of spheres as nanoplankton previously thought to only be free living.

Recently, coleoid cephalopods were shown to have ordered microprojections on their corneas, but researchers suggested that their size (heights of less than 60 nm) and low refractive index (1.40) did not function in enhancing crypsis [25] because of the small index difference between seawater and their cornea. Even with the slightly larger index difference between chitin and seawater, we similarly found that the 52 nm spheres were less effective than other sizes at reducing reflectance.

We performed additional calculations to determine the optimal thickness and effective index of a monolayer of spheres for a relevant optical situation that these hyperiids may encounter—downward blue light striking the body at a 45° angle and being reflected horizontally (Figure 4A). If we assume the spheres are bacteria with an index of 1.44 [22] and we assume that the spheres are confluent, then the greatest reduction in the intensity of overhead blue light (480 nm) that is reflected horizontally occurs when the spheres have diameters of approximately 110 nm. Reducing bacterial density by half lowered the effective index to approximately 1.39, which caused the reduction in reflectance to change from 250-fold to 4-fold (Figure 4A). However, even a 4-fold reduction in reflectance under certain viewing conditions may be enough to benefit a hyperiid attempting to evade detection. Although we only consider surface reflectance and not internal scattering, the calculated Weber contrasts of a hyperiid cuticle with and without the cuticular nanostructures and spheres show that the cuticular features decrease the reflectance of downwelling light enough to make a difference in the visibility of the cuticle (Figure 4B). We suggest that future work on surface structures and colonizing organisms should consider the potential optical effects of these features by testing reflectance predictions and measuring whole-body scattering in living animals.

SUPPLEMENTAL INFORMATION

Supplemental Information includes Supplemental Experimental Procedures and three figures and can be found with this article online at http://dx.doi.org/10.1016/j.cub.2016.09.033.

AUTHOR CONTRIBUTIONS

Conceptualization, L.E.B.; Methodology for Microscopy and Optical Models, S.J. and L.E.B.; Investigation, L.E.B.; Resources, K.J.O.; Writing – Original Draft, L.E.B. and S.J.; Writing – Review & Editing, L.E.B., S.J., and K.J.O.; Funding Acquisition, S.J. and L.E.B.

ACKNOWLEDGMENTS

We thank three anonymous reviewers; Eleanor Caves; Kate Thomas; Benjamin (Jay) Wheeler; and Drs. Jamie Baldwin Fergus, Dan Speiser, Robert Fitak, Lorian Schweikert, and Nicholas Brandley for comments on earlier versions of this manuscript. We thank Richard Dillaman and Mark Gay (UNC Wilmington), Michelle Gignac (Duke's Shared Materials Instrumentation Facility), and Scott Whittacker (Smithsonian) for assistance with electron microscopy. We also thank the affiliates of the *RV Endeavour*, *RV Kilo Moana*, *RV Western Flyer*, and *RV Sunburst* for facilitating specimen collection. Funding was provided

by grants from the National Science Foundation (OCE-0852138) and Office of Naval Research (N00014-09-1-1053) to S.J. and Sigma Xi Grant-in-Aid of Research and Rathbun Crustacean Research Endowment at Smithsonian NMNH to L.E.B.

Received: May 13, 2016
Revised: August 8, 2016
Accepted: September 16, 2016
Published: October 27, 2016

REFERENCES

1. Chapman, G. (1976). Reflections on transparency. In Coelenterate Ecology and Behavior, G.O. Mackie, ed. (Plenum Press), pp. 491–498.
2. Greze, V.N. (1963). The determination of transparency among planktonic organisms and its protective significance. Dokl. Akad. Nauk SSSR *151*, 435–438.
3. Johnsen, S. (2001). Hidden in plain sight: the ecology and physiology of organismal transparency. Biol. Bull. *201*, 301–318.
4. Mackie, G.O. (1996). Defensive strategies in planktonic coelenterates. In Zooplankton: Sensory Ecology and Physiology, P.H. Lenz, D.K. Hartline, J.E. Purcell, and D.L. Macmillan, eds. (Overseas Publishers Association), pp. 435–446.
5. Johnsen, S. (2003). Lifting the cloak of invisibility: the effects of changing optical conditions on pelagic crypsis. Integr. Comp. Biol. *43*, 580–590.
6. Johnsen, S. (2011). The Optics of Life: A Biologist's Guide to Light in Nature (Princeton University Press), pp. 116–150.
7. Zylinski, S., and Johnsen, S. (2011). Mesopelagic cephalopods switch between transparency and pigmentation to optimize camouflage in the deep. Curr. Biol. *21*, 1937–1941.
8. Chattopadhyay, S., Huang, Y.F., Jen, Y.J., Ganguly, A., Chen, K.H., and Chen, L.C. (2010). Anti-reflecting and photonic nanostructures. Mater. Sci. Eng. Rep. *69*, 1–35.
9. Raut, H.K., Ganesh, V.A., Nair, A.S., and Ramakrishna, S. (2011). Anti-reflective coatings: a critical, in-depth review. Energy Environ. Sci. *4*, 3779–3804.
10. Bowman, T.E., and Gruner, H.E. (1973). The families and genera of Hyperiidea (Crustacea: Amphipoda). Smithson. Contrib. Zool. *146*, 1–60.
11. Vinogradov, M.E., Volkov, A.F., Semenova, T.N., and Siegel-Causey, D. (1996). Hyperiid Amphipods (Amphipoda, Hyperiidea) of the World Oceans (Science Publications).
12. Bernhard, C.G., and Miller, W.H. (1962). A corneal nipple pattern in insect compound eyes. Acta Physiol. Scand. *56*, 385–386.
13. Stoddart, P.R., Cadusch, P.J., Boyce, T.M., Erasmus, R.M., and Comins, J.D. (2006). Optical properties of chitin: surface-enhanced Raman scattering substrates based on antireflection structures on cicada wings. Nanotechnology *17*, 680–686.
14. Dobrowolski, J.A. (1995). Optical properties of films and coatings. In Handbook of Optics, M. Bass, ed. (McGraw-Hill), pp. 42.3–42.130.
15. Johnsen, S. (2002). Cryptic and conspicuous coloration in the pelagic environment. Proc. Biol. Sci. *269*, 243–256.
16. Stavenga, D.G., Foletti, S., Palasantzas, G., and Arikawa, K. (2006). Light on the moth-eye corneal nipple array of butterflies. Proc. Biol. Sci. *273*, 661–667.
17. Yoshida, A., Motoyama, M., Kosaku, A., and Miyamoto, K. (1996). Nanoprotuberance array in the transparent wing of a hawkmoth, *Cephanodes hylas*. Zoolog. Sci. *13*, 525–526.
18. Siddique, R.H., Gomard, G., and Hölscher, H. (2015). The role of random nanostructures for the omnidirectional anti-reflection properties of the glasswing butterfly. Nat. Commun. *6*, 6909.
19. Dellieu, L., Sarrazin, M., Simonis, P., Deparis, O., and Vigneron, J.P. (2014). A two-in-one superhydrophobic and anti-reflective nanodevice in the grey cicada *Cicada orni* (Hemiptera). J. Appl. Phys. *116*, 024701.
20. Cai, J., and Qi, L. (2015). Recent advances in antireflective surfaces based on nanostructure arrays. Mater. Horiz. *2*, 37–53.
21. Gusnard, D., and Kirschner, R.H. (1977). Cell and organelle shrinkage during preparation for scanning electron microscopy: effects of fixation, dehydration and critical point drying. J. Microsc. *110*, 51–57.
22. Stramski, D., Bricaud, A., and Morel, A. (2001). Modeling the inherent optical properties of the ocean based on the detailed composition of the planktonic community. Appl. Opt. *40*, 2929–2945.
23. Chao, Y., and Zhang, T. (2011). Optimization of fixation methods for observation of bacterial cell morphology and surface ultrastructures by atomic force microscopy. Appl. Microbiol. Biotechnol. *92*, 381–392.
24. Wagner, H.J., Fröhlich, E., Negishi, K., and Collin, S.P. (1998). The eyes of deep-sea fish. II. Functional morphology of the retina. Prog. Retin. Eye Res. *17*, 637–685.
25. Talbot, C., Jordan, T.M., Roberts, N.W., Collin, S.P., Marshall, N.J., and Temple, S.E. (2012). Corneal microprojections in coleoid cephalopods. J. Comp. Physiol. A Neuroethol. Sens. Neural Behav. Physiol. *198*, 849–856.

Current Biology, Volume *26*

Supplemental Information

Nanostructures and Monolayers of Spheres Reduce Surface Reflections in Hyperiid Amphipods

Laura E. Bagge, Karen J. Osborn, and Sönke Johnsen

Supplemental Figures

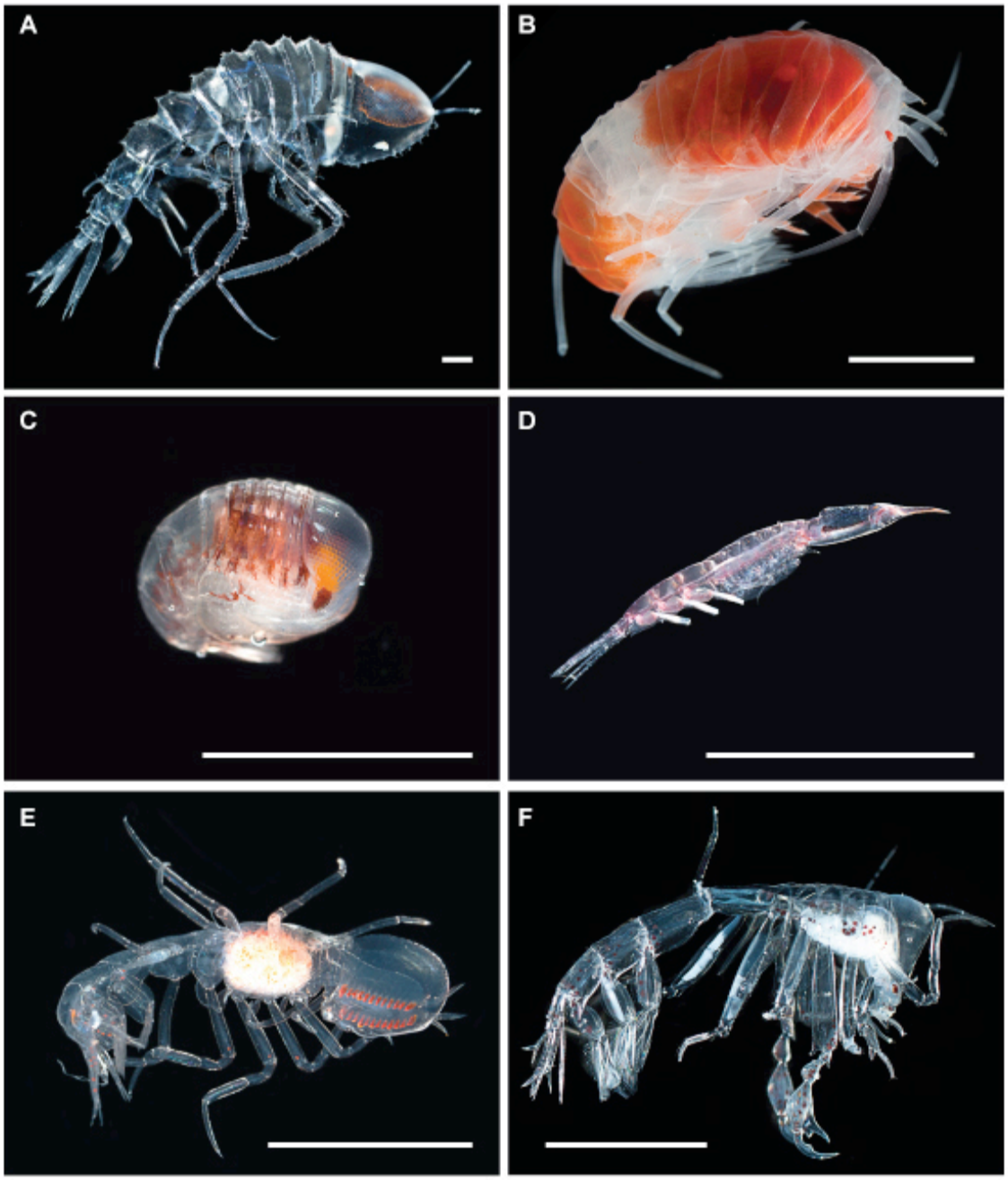

Figure S1. Exemplar hyperiids. Related to Figure 1.
(A) Cystisomatidae, *Cystisoma.* (B) Lanceolidae, *Lanceola*.
(C) Platyscelidae, *Platyscelus*. (D) Oxycephalidae, *Leptocotis*.
(E) Paraphronimatidae, *Paraphronima crassipes*. (F) Phronimatidae, *Phronima sedentaria*. Scale bars are 5 mm. Note that photographs were taken *ex situ* using four xenon flashes mounted on the four sides of the holding tank to maximize the visibility of the animal.

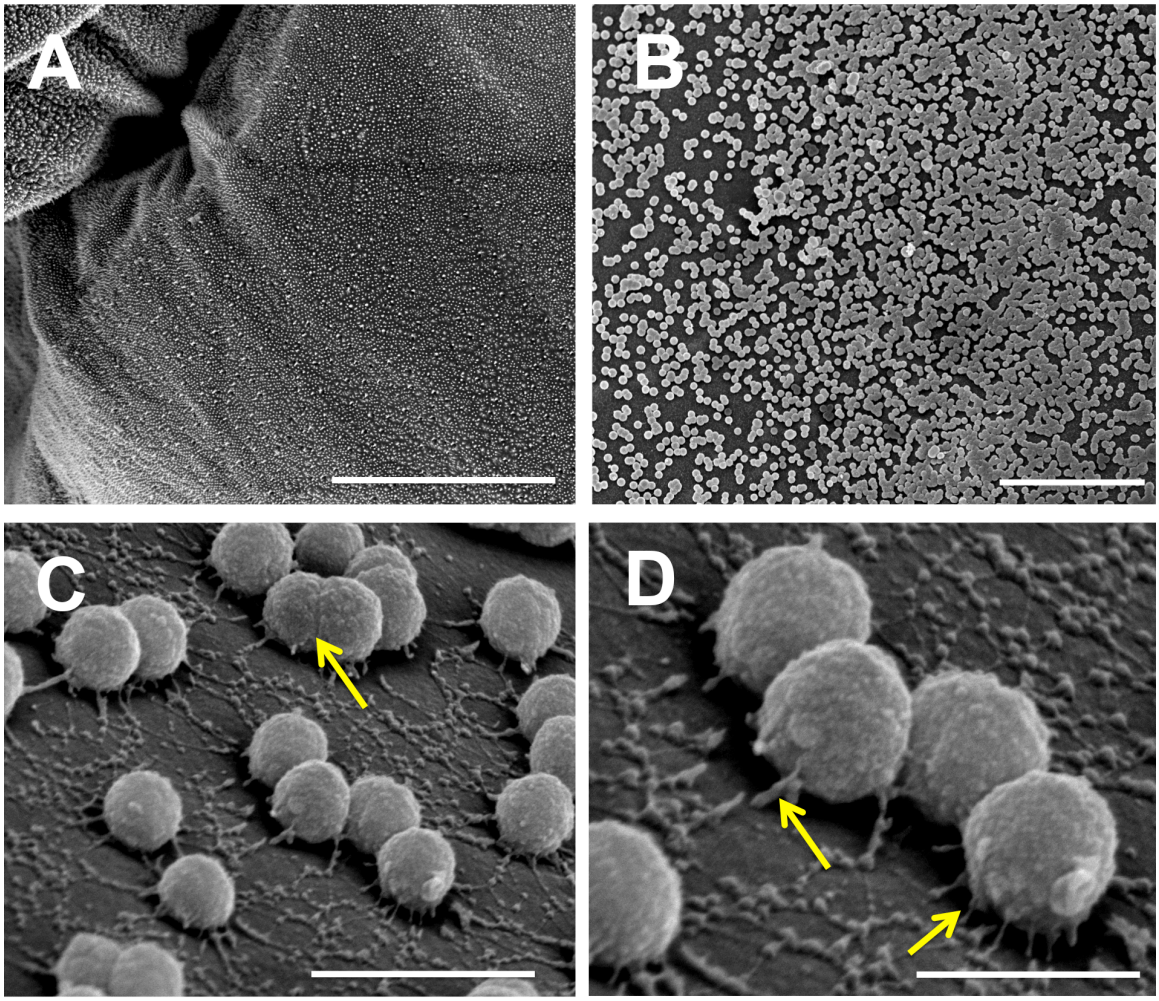

Figure S2. Scanning electron micrographs of the surfaces of hyperiids. Related to Figure 1. (A) Example micrograph demonstrating that nanoprotuberances cover the appendages from the insertion (shown) to the distal tip on *Cystisoma* spp. Scale bar is 10 µm. **(B)** Example micrograph showing variability in sphere coverage on the dorsal surface of one *Phronima* specimen. Scale bar is 10 µm. **(C)** Evidence that the spheres on *Phronima* are nanobacteria. The yellow arrow shows what appears to be a plane of division. Scale bar is 1 µm. **(D)** Yellow arrows show that the spheres are attached to the cuticle surface with what appear to be fimbrae. Scale bar is 500 nm.

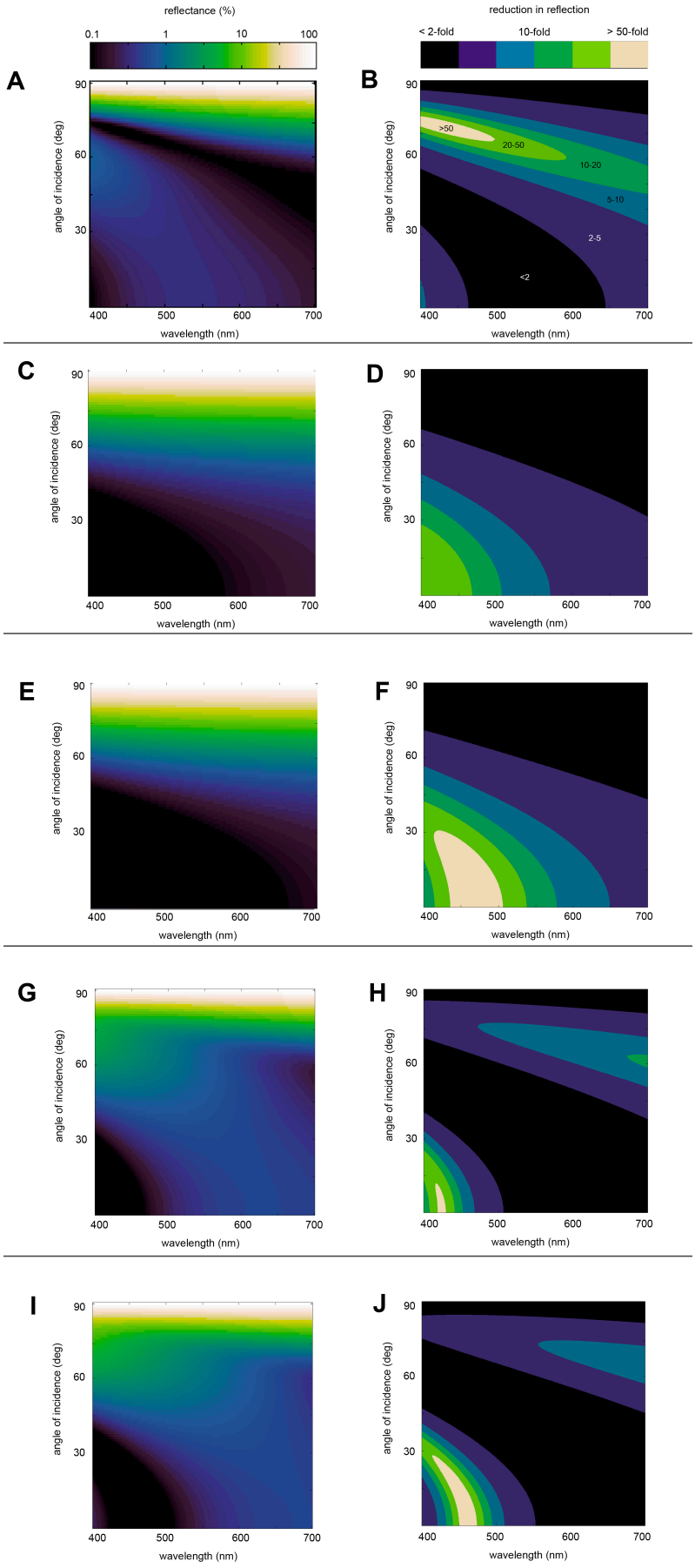

Figure S3 (Left) Transfer matrix predictions (related to Figure 3) of cuticle reflectance in seawater and (Right) the reduction in reflection as compared to a clean, flat chitinous cuticle for **(A-B)** the nanoprotuberances on *Cystisoma* appendages, 20% wider (accounting for possible shrinkage during SEM preparation); **(C-D)** the 70 nm thick layer found on the cuticle of *Lanceola*; **(E-F)** the 80 nm layer found on the cuticle of *Platyscelus*; **(G-H)** the 220 nm layer found on the cuticle of *Glossocephalus*; and **(I-J)** the 240 nm layer found on the cuticle of *Paraphronima*.

Supplemental Experimental Procedures

Specimen collection

Hyperiid amphipods were collected using an opening-closing midwater trawl with a thermally insulated cod-end [S1] at 100-1,000 m depth. Collection sites included: Oceanographer's Canyon in the North Atlantic from the *RV Endeavor* in September 2011; off the western coast of the big island of Hawaii in the Pacific from the *RV Kilo Moana* in June 2012; Monterey Submarine Canyon in the eastern Pacific from the *RV Western Flyer* from 2011-2014, and in the northwestern Atlantic off the coast of Ft. Pierce, FL from the *R/V Sunburst* in August 2014. Specimens were also examined from the Crustacean Collection at the Smithsonian National Museum of Natural History. Freshly collected animals were fixed for a minimum of 48 hours in 2.5% glutaraldehyde in Sorensen's phosphate buffer for later examination by microscopy.

Examination of cuticular surface using electron microscopy

Specimens were first placed in phosphate buffered saline and then taken through a graded ethanol dehydration series and dried using hexamethyldisilazane (HMDS). Dried specimens were coated with platinum/palladium (80/20) using a Cressington 208 HR sputter coater and examined using a Philips XL30S FEG SEM, with preliminary scans performed at approximately 5,000x magnification. Areas of interest were further magnified from 10,000x to 150,000x, and images were captured and later analyzed using Fiji, an open-source platform for image analysis [S2].

Modeling surface reflectance

We measured the heights, widths and spacings of 100 randomly sampled nanoprotuberances from different regions of the pereopods of two specimens of *Cystisoma* using the image analysis tool Fiji [S2]. Additionally, because the tips of the structures had a smaller width than the bases, we took at least six width measurements at different heights for each nanoprotuberance. We then calculated the fractional area of the chitinous structures at every height above the surface of the main cuticle, which allowed us to calculate the effective refractive index (n_{eff}) using the equation:

$$n_{eff} = \sqrt{A_{chitin} n_{chitin}^2 + A_{water} n_{water}^2}$$

where A is the fractional area ($A_{chitin} + A_{water} = 1$) and n is the real refractive index. The refractive indices of chitin and seawater vary slightly with wavelength over the visible range, but average approximately 1.57 and 1.34 [S3, S4, S5]. We accounted for this wavelength dependent variation using the Cauchy equations [S6 and S7]:

$$n_{water} = 1.3205 + \frac{5201}{\lambda^2} \qquad n_{chitin} = 1.517 + \frac{8800}{\lambda^2}$$

We then input the effective indices into a transfer matrix model to calculate reflectance from a stack of 40 layers, each 5 nm in thickness (see Transfer Matrix Model below). The reflectance from the monolayers of spheres was calculated using the same transfer matrix model, but instead of multiple layers, the spheres were input as a single layer of refractive index 1.44 [S5].

Transfer matrix model

The fraction of light, *R*, reflected from a stack of *L* thin layers overlaying a substrate is given by:

$$R = |r|^2 ,$$

where *r* is the amplitude reflection coefficient, which is equal to:

$$r = \frac{\eta_m E_m - H_m}{\eta_m E_m + H_m} .$$

E_m and H_m are the electric and magnetic fields of the reflected light in the external medium (in this case, water) with an effective index η_m and are found by multiplying a set of matrices, one for each layer:

$$\begin{pmatrix} E_m \\ H_m \end{pmatrix} = \mathbf{M} \begin{pmatrix} 1 \\ \eta_s \end{pmatrix}, \text{ where } \mathbf{M} = \mathbf{M_L M_{L-1} ... M_2 M_1} \text{ and}$$

$$\mathbf{M}_j = \begin{pmatrix} \cos\delta_j & \frac{i}{\eta_j}\sin\delta_j \\ i\eta_j \sin\delta_j & \cos\delta_j \end{pmatrix} .$$

The optical pathlength δ for the j^{th} layer is:

$$\delta_j = \frac{2\pi}{\lambda} n_j d_j \cos\theta_j .$$

The effective refractive index η equals $n\cos\theta$ for parallel polarization and $n/\cos\theta$ for perpendicular polarization, where θ is the angle of incidence of the light in the medium, layer, or substrate (underlying cuticle) and is given by Snel's law:

$$n_m \sin\theta_m = n_j \sin\theta_j = n_s \sin\theta_s .$$

$n_{m,j,s}$	real refractive index of external medium, layer, or substrate
d_j	thickness of layer *j*
$\theta_{m,j,s}$	angle of incident and reflected light measured from the perpendicular to the surface in external medium, layer, or substrate
λ	wavelength of incident light (in a vacuum)
m	subscript for medium (water)
j	subscript for a given layer
s	subscript for substrate (underlying cuticle)
i	the square root of -1

Supplemental References

S1. Childress, J.J., Barnes, A.T., Langdon, B.Q., and Robison, B.H. (1978). Thermally protecting cod ends for the recovery of living deep-sea animals. Deep-Sea Res. *25*, 419-422.

S2. Schindelin, J., Arganda-Carreras, I., Frise, E., Kaynig, V., Longair, M., Pietzsch, T., Preibisch, S., Rueden, C., Saalfeld, S., Schmid, B., et al. (2012). Fiji: an open-source platform for biological-image analysis, Nat. Methods *9*, 676-682.

S3. Berhard, C. G., and Miller, W.H. (1962). A corneal nipple pattern in insect compound eyes. Acta Physiol. Scand. *56*, 385-386.

S4. Stoddart, P.R., Cadusch, P.J., Boyce, T.M., Erasmus, R.M., and Comins, J.D. (2006). Optical properties of chitin: surface-enhanced Raman scattering substrates based on antireflection structures on cicada wings. Nanotechnology *17*, 680-686.

S5. Stramski, D., Bricaud, A., and Morel, A. (2001). Modeling the inherent optical properties of the ocean based on the detailed composition of the planktonic community. Appl. Opt. *40*, 2929-2945.

S6. Bashkatov, A.N., and Genina, E.A. (2002). Water refractive index in dependence on temperature and wavelength: a simple approximation. Proc. SPIE *5068*, 393-395.

S7. Leertouwer, H.L., Wilts, B.D., and Stavenga, D.G. (2011). Refractive index and dispersion of butterfly chitin and bird keratin measured by polarizing interference microscopy. Opt. Express *19*, 24061-24066.